Nuclear Instruments and Methods in Physics Research A 343 (1994) 292–299
North-Holland

NUCLEAR
INSTRUMENTS
& METHODS
IN PHYSICS
RESEARCH
Section A

The DIRC counter: a new type of particle identification device for B factories **

P. Coyle [a,*], H. Kawahara [b], A. Lu [c], G. Lynch [d], G. Mueller [b], D. Muller [b], B. Ratcliff [b], C. Simopoulos [b]

[a] *Centre de Physique des Particules de Marseille, Luminy, 13288 Marseille, France*
[b] *Stanford Linear Accelerator Center, Stanford University, Stanford, CA 94309, USA*
[c] *Department of Physics, University of California, Santa Barbara, CA 93106, USA*
[d] *Lawrence Berkeley Laboratory, University of California, Berkeley, CA 94720, USA*

A very thin, solid radiator, totally internally reflecting, imaging Cherenkov counter (DIRC) is described. This device is well matched to the hadronic charged particle identification requirements at an asymmetric e^+e^- B factory.

1. Introduction

Particle identification at a B factory is difficult [1]; good pion/kaon separation is required over a wide momentum range between about 0.25 and 4 GeV/c. In addition, the amount of material in the device should be small (preferably less than 10% X_0) and be distributed as close as possible to the calorimeter in order to avoid degradation in the resolution performance of the calorimeter, and the loss of low energy conversion electrons in the magnetic field [2]. Also, as the cost of the high quality calorimeter scales roughly as the radius squared, there will be substantial cost savings if the particle identification device can be made thin.

Here, we describe a new type of imaging Cherenkov (the DIRC, for Detection [of] Internally Reflected Cherenkov [light]) that appears to be extremely well matched to the requirements for particle identification at the B factory. It is thin (with low radiation length), robust, very fast, and should have excellent performance over the complete phase space of the B factory. Although many configurations of a DIRC type device are possible, for definiteness, a particular model will be discussed which uses quartz radiator bars, read out by conventional photomultiplier tubes in a proximity focused geometry. A brief discussion of some possible variations will follow within the space limitations here. More details can be found elsewhere [3].

* Corresponding author.
** Work Supported by Department of Energy contract DE-AC03-765F00515.

2. The DIRC imaging principle

The geometry of a single radiator of the DIRC is shown schematically in Fig. 1. Each radiator is a long, thin, flat "bar" with rectangular cross section [t_x, t_y]. There is a photodetection surface positioned some distance (l) away from the end of the bar. A track with velocity β passing through the radiator with refractive index n_1 emits Cherenkov radiation in a cone around the particle trajectory.

The angles, positions, and momentum of the track are provided by a tracking device located in front of the radiator. If the index of refraction of the radiating material (n_1) substantially exceeds $\sqrt{2}$, and n_3 is approximately 1, then, for a particle close to $\beta = 1$, some portion of the light will always be transported down the "bar" to the end. Since the radiator cross-section is rectangular, angles are maintained in reflections at the surfaces of the bar (up to an additional up–down/left–right ambiguity). Thus, in a perfect bar, the portion of the Cherenkov cone that lies inside the total internal reflection angle is transported undistorted down the bar to the end. When it reaches the end, the light either reflects or emerges into a standoff region with index n_2. It then travels some distance until it hits a two dimensional detection surface, where it forms an image on the surface as shown in Fig. 2. The image is essentially a conic section of the cone – suitably modified by refraction at the n_1, n_2 interface. It has been "doubled" because of the up–down reflection ambiguity. In the case shown, the track enters the radiator in the y–z plane so that the left and right going images are symmetrical. Since the locus of the image depends

SSDI 0168-9002(93)E1174-V

on the polar and azimuthal Cherenkov angles (θ_C, ϕ_C), particle identification using Cherenkov angular information can proceed using essentially the same hypothesis testing techniques employed by imaging Cherenkov devices of the RICH/CRID type [4].

Four different image loci are shown in Fig. 2 corresponding to different extremes for the width t_x of the bar, as shown schematically in Fig. 1. In the extreme limit of the PLATE geometry, the bar is sufficiently wide that no reflections occur from the sides of the bar, and there is no left–right imaging ambiguity. In the other limit, the PIPE geometry, the bar width t_x is much smaller than the photon measurement resolution, and there is complete left–right overlap. The PLATE geometry has fewer ambiguities in the case where it is geometrically feasible to make the plate very wide (perhaps in a fixed target environment), but it does not seem possible to devise a full acceptance counter for a solenoidal detector at a collider without a significant number of photon bounces from the sides. Unless the PLATE has a large width/length ratio, the image depends in detail on the number of bounces, the width of the radiator, the position of the track in the radiator bar, etc., and consists of a number of disconnected pieces as shown in Fig. 2c. We thus prefer to image using the PIPE geometry and to accept the left–right imaging ambiguity implied. Then, in the limit of infinite transmission coefficient and small pipes, the observed image is dependent only on the track velocity and angles with respect to the bar, and independent of position in the bar [5].

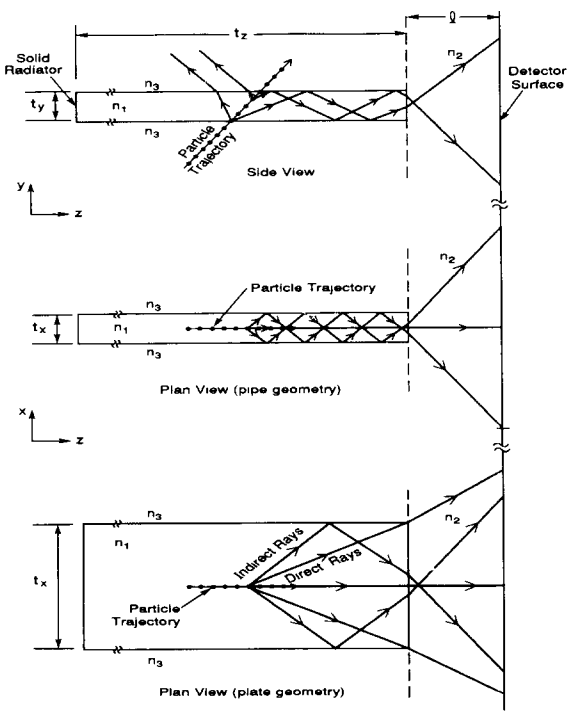

Fig. 1. Schematic of a radiator bar of the DIRC counter for two different radiator widths (pipe and plate) described in the text; the particle trajectory is shown as a line connected by dots; representative trajectories of Cherenkov photons are shown by lines with arrows.

Not all the Cherenkov photons produced in the radiator can be collected by the detector. Some photons are produced at angles below the total internal reflection limit and emerge from the faces of the radiator while others can essentially be trapped in the radiator bar and are lost. This is illustrated in Fig. 3 which gives an accounting of the fate of the photons within the bar as a function of the dip angle for a $\beta = 1$ track. It is clear that for dip angles close to 0° and 90° the transfer efficiency is rather small.

One method to improve the transfer efficiency is to fill the standoff region between the radiator and the detector with a material whose index is substantially higher than 1.0. In particular, if the standoff region is filled with a material with the same index as the radiator (i.e. $n_1 = n_2$), then the transfer efficiency is maximized and the images will emerge without reflection or refraction at the end surface.

Fig. 4 shows the Cherenkov photon transport efficiency as a function of the index (n_2) of the standoff region. In the case that the radiator and standoff region have the same index, the nominal transmission exceeds 45% for all angles when β exceeds 0.93, which corresponds to $P_\pi = 0.35$, and $P_K = 1.24$ GeV/c. Below 1.24 GeV/c, a DIRC with these parameters will function as a threshold Cherenkov for p/K separation over the central part of the angular acceptance, and will be unable to distinguish kaons from protons there.

3. The radiator

For a solenoidal geometry, the radiators must have very long Cherenkov photon absorption length and high quality surface finish (for good transmittance down the bar); flat, orthogonal surfaces (for accurate image transmission); low chromatic dispersion (to allow a good measurement of the Cherenkov angle); appropriate index of refraction (to transmit light down the bar); and preferably, long radiation length. Though a short device could be built using one of the fluoride glasses (e.g., LiF or CaF_2) operating in the TMAE regime, we know of no material suitable for operation of a long device (e.g., 2–6 m) in the 1700–2000 Å region where TMAE is sensitive. The "obvious" radiator choice for a long device is quartz, working in the visible to near UV range (i.e., 3000–6000 Å). As shown in Fig. 5, it has a transmission length which exceeds 50 m over most of this wavelength range; it takes a high quality polish so that internal reflection coefficients can be made high;

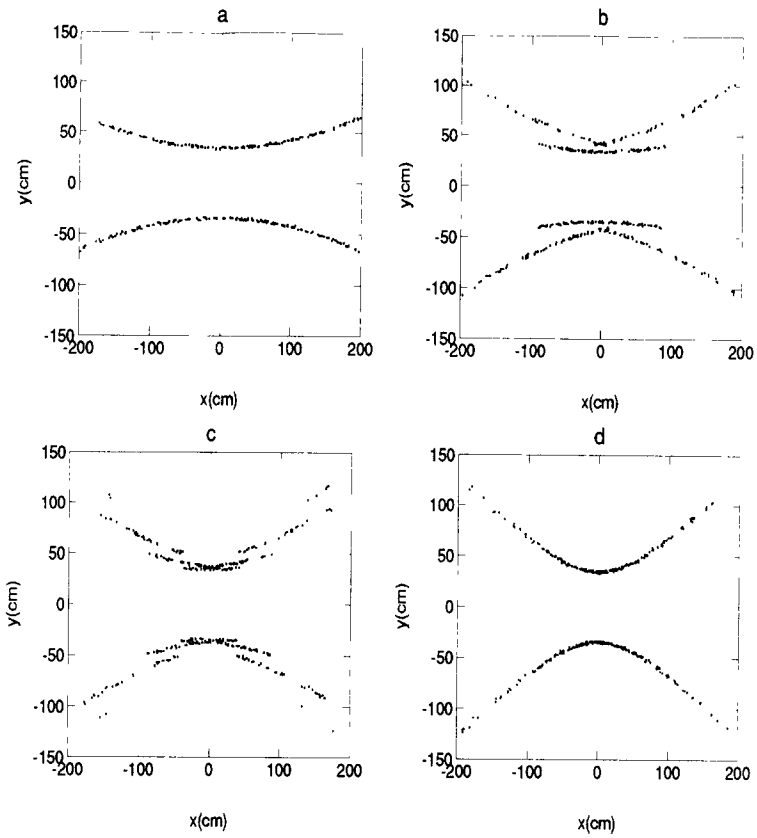

Fig. 2. Loci of images for a $\beta = 1$ track at a dip angle of 30° for radiator widths of (a) $t_x = 1000$ cm (b) $t_x = 100$ cm (c) $t_x = 20$ cm (d) $t_x = 5$ cm. The track azimuthal angle (dx/dy) is zero. The radiator is quartz ($\langle n_1 \rangle = 1.474$) and the detector standoff regions is air ($n_2 = 1.0$). The distance of the detector from the radiator is 100 cm. The track enters at $t_x/2$ and at 100 cm from the end of the 1 cm thick radiator.

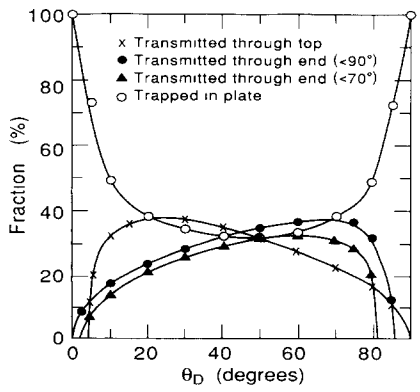

Fig. 3. An accounting of the fate of the photons in a quartz radiator ($\langle n_1 \rangle = 1.474$) as a function of the dip angle for a $\beta = 1$ track. The standoff region is air ($n_2 = 1.0$). The open circles indicate that a large fraction of the light is trapped, especially near 0° and 90°. In this simple model effects from absorption and scattering have been neglected.

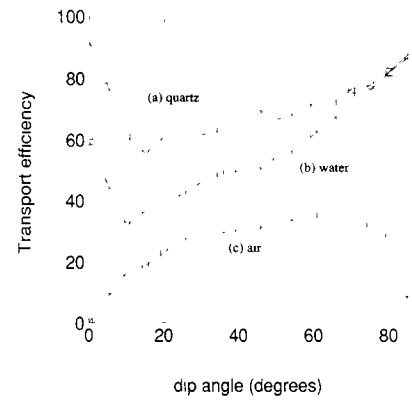

Fig. 4. The fraction of Cherenkov photons transmitted to the detector as a function of dip angle for various refractive indices in the standoff region: (a) quartz ($n_2 = 1.474$), (b) water ($n_2 = 1.34$) and (c) air ($n_2 = 1.0$). The radiator is quartz ($\langle n_1 \rangle = 1.474$). Note the improvement in efficiency for small dip angles as n_2 approaches n_1. In this simple model, effects from absorption and scattering have been neglected.

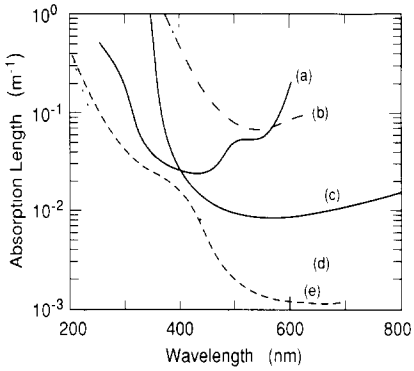

Fig 5. Examples of absorption lengths as a function of wavelength for some potential radiator and standoff region materials: (a) water (IMB quality) [6], (b) UVT acrylic [7], (c) laser liquid 3421 [8], (d) fused silica fiber [9], (e) bulk fused silica [10].

it has the lowest dispersion of the oxide glasses (Abbe number 67.8); and it can be procured in large pieces at relatively modest cost.

The refractive index (n_2) of the standoff region material between the detector and the radiator bar should be well matched to that of the radiator and should have a rather long absorption length. It could be the same material as the radiator bar, but in the case of quartz, it seems more likely that the region would be filled with a liquid. Though there are liquid materials available which match the refractive index of quartz extremely well, their transmission in the near UV tends to be inadequate. Fig. 5 shows the response of two candidate liquids which do have reasonable UV transmissions, curves (b) for water ($n_2 = 1.34$), and (c) for Cargille labs laser liquid 3421 ($n_2 = 1.41$). Water is inexpensive and quite transparent over the required range but would lead to some modest reflective losses at the n_1, n_2 interface for large angles. Liquid 3421 has a somewhat better refractive index match but cuts off earlier in wavelength, which would reduce the effective N_0.

For the rest of this paper, we will assume that the radiator bars are made of quartz with index of refraction $n_1 = 1.474$, when weighted by the Cherenkov spectrum and the photodetector response, and for simplicity will also assume that $n_1 = n_2$. Other alternatives are discussed elsewhere [3].

4. The photodetector

The number of Cherenkov photons produced and transmitted to the detector surface is generally small, so it is important to obtain good efficiency from the photodetector. Moreover, since the position of each photon must be detected, the single photon signal-to-noise ratio must be very good. The photodetector surface must be some minimum distance away from the radiator end (to obtain adequate resolution). Finally, the detector should be rather fast. The "classic" device which fulfills these conditions is the photomultiplier tube, and a photodetection surface can be made of an array of these tubes with a packing fraction typically of about 66%. This also has the conceptual "advantage" that the detector uses completely "conventional" technology whose performance is well understood and can be reliably simulated. In addition, the good timing resolution of a PMT will also provide modest spatial resolution (~ 10 cm for a typical PMT) along the bar, which is useful to reject background, and to determine the emission direction of the photon if a reflective surface is used on one end. Alternatively, the timing provides a measure of the photon path length to the photodetector. Since this depends on the light propagation angles, and production point in the bar, it provides an independent measure of a particular convolution of the Cherenkov angles, which could be useful to improve the angle measurement in some cases, if the photon detector is very fast [11].

5. Model for B factory detector

In this section, we will describe a particular model of a B factory detector which incorporates a DIRC. Many of the geometrical details of such a detector are arbitrary and a great many different configurations are clearly possible.

A view of the forward quadrant of this "model" B factory detector is shown in Fig. 6. In order to avoid the difficult problem of keeping the end plate masses

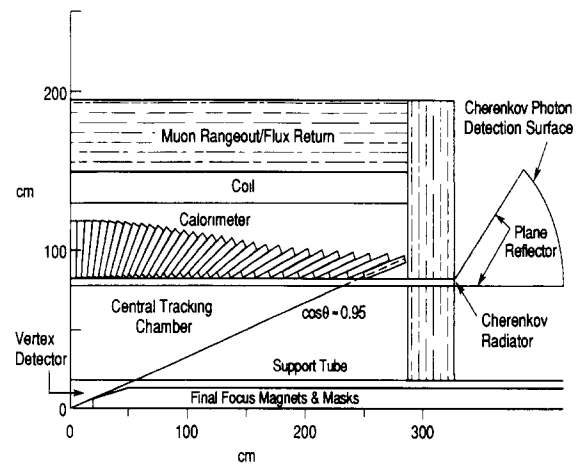

Fig. 6. Schematic view of one quadrant of a B factory detector incorporating a DIRC.

low in the central tracking devices, the particular geometry shown has no end caps. This also allows very uniform calorimetry and the simplest possible DIRC geometry. The "stretched" geometry is particularly attractive in this case because the inner radius of the calorimeter is so small. It is assumed that the DIRC radiator consists of $1.23 \times 4.0 \times 560$ cm (t_x, t_y, t_z) quartz bars. The radiator is 10% X_0 thick radially and takes up to about 2.5 cm of radial space in all. The bars are placed on a 20 sided polygonal surface, as viewed from the end of the detector, and cover about 98% of the azimuth. The detectors are closely packed arrays of conventional photomultiplier (PMT) tubes at each end. As shown in Fig. 6, the surface is a cylindrical section in elevation and approximately toroidal as viewed from the end. The detector boxes have reflecting surfaces at the inner polygonal surface (approximately in the radiator x–z plane) and at $\tan^{-1} \mathrm{d}y/\mathrm{d}z = 1$ to save phototubes. They are filled with a fluid whose refractive index matches that of quartz, so there are no reflections at the radiator ends or phototube windows. The device works in the near ultraviolet and the visible. It is thin and compact, robust, very fast, and self-triggering.

The loci of Cherenkov images on a cylindrical detector surface for $\beta = 1$ tracks at a number of different dip angles are shown in Fig. 7 for the case where the track enters the radiator bar perpendicularly in azimuth. The images at the detector for a particular dip angle ($\theta_D = 30°$) are shown in Fig. 8 for three different angles in azimuth. One can see that for azimuthal angles other than zero, the images are "doubled" due to the side edge reflection.

6. Simple performance model

In this section, we will discuss a simple model for the performance of a DIRC counter such as that described above to elucidate some of the important issues which determine the performance. The number of photoelectrons (N_{PE}) produced in the photodetector can be written as:

$$N_{PE} = \frac{\epsilon N_0 L \sin^2\theta_C}{\cos \theta_D},$$

where N_0 is the Cherenkov quality factor (about 100 cm^{-1} for a good bialkali phototube), L is the radial radiator thickness ($L = t_y = 1.23$ cm), and ϵ is the total collection efficiency. Sin θ_C for a $\beta = 1$ particle in quartz equals 0.735. ϵ can be thought of as being composed of two main pieces. The first is the geometrical photon transport efficiency down the bar, through

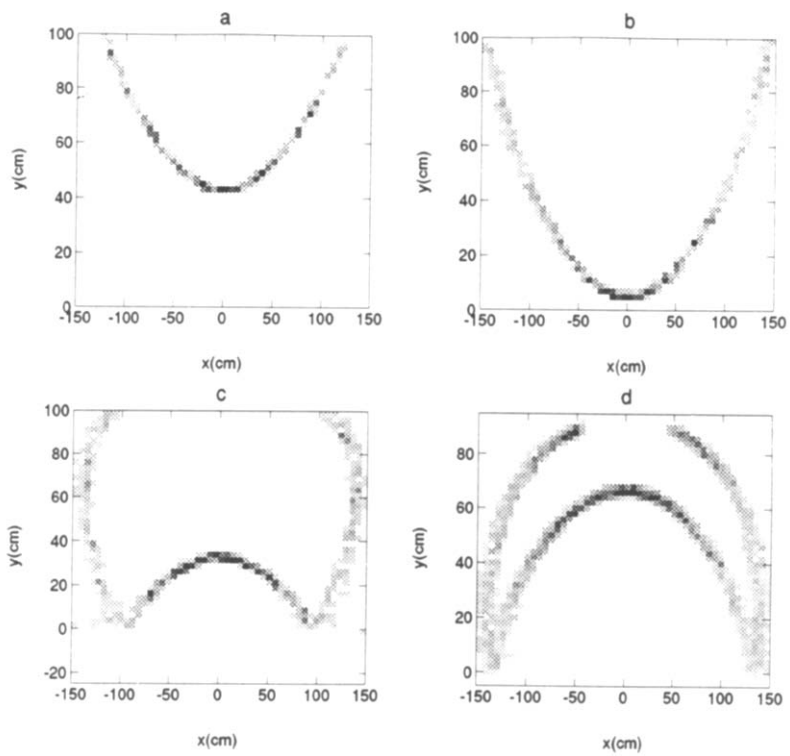

Fig. 7. Loci of Cherenkov images from a $\beta = 1$ track on a cylindrical detection surface 100 cm from the radiator end. The track enters the radiator perpendicularly in azimuth. Dip angles of (a) 20°, (b) 40°, (c) 60° and (d) 80° are shown.

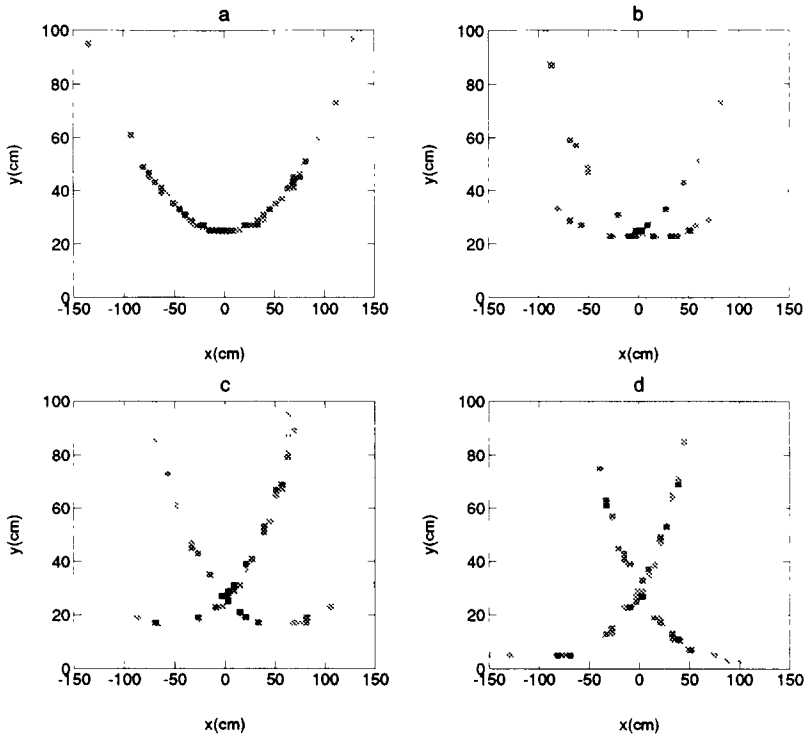

Fig. 8. Loci of Cherenkov images from a $\beta = 1$ track on a cylindrical detection surface 100 cm from the radiator end. The track is at a dip angle (θ_D) of 30° and images are shown for four different azimuthal angles (a) 0°, (b) 10°, (c) 20° and (d) 30°.

the n_1–n_2 interface, to the photodetector. This efficiency is a strong function of track dip angle and the azimuthal acceptance for photons in the bar. Second, closely packed PMTs only cover about 66% of the surface with an active photocathode, and it is difficult to increase the efficiency much by collection optics given the large acceptance requirements.

The number of photoelectrons N_{PE} expected for a $\beta = 1$ particle as a function of dip angle is shown in Table 1.

The total separation in Cherenkov angle $\delta\theta_C(\text{tot})$ is given by

$$\delta\theta_C(\text{tot}) = \delta\theta_C/\sqrt{N_{PE}}\,,$$

Table 1
The number of photoelectrons expected for a $\beta = 1$ particle as a function of dip angle

θ_D	N_{PE}
0	27
15	17
30	22
50	56
70	83

where the angular error measurement from each photon detected $\delta\theta_c$ is the sum in quadrature of the following terms:

$-\delta\theta_{\text{Production}}$: Each of these terms include a number of contributions. The error associated with the Cherenkov photon production process $\delta\theta_{\text{Production}}$ is dominated by chromatic dispersion $\delta\theta_{\text{Chromatic}}$, and also includes contributions from multiple scattering $\delta\theta_{\text{MS}}$, and momentum bending in the radiator, $\delta\theta_{\text{Momentum}}$. Dispersion in the radiator is the "fundamental" performance limit on attainable performance in an imaging Cherenkov. It is given by

$$\delta\theta_{\text{Chromatic}} = \frac{1}{\tan\theta_C}\frac{dn}{n}. \tag{5}$$

Thus, the chromatic dispersion contribution depends on the radiator dispersion averaged over the response of the photodetector. For a DIRC with a quartz radiator and bialkali photocathodes, this averaged value of dn/n is 5.8 mrad, so that $\delta\theta_{\text{Chromatic}}$ is 5.4 mrad for a $\beta = 1$ particle. The errors associated with $\delta\theta_{\text{MS}}$ and $\delta\theta_{\text{Momentum}}$ are quite small and can be ignored.

– $\delta\theta_{\text{Transport}}$: The smearing of the Cherenkov photons in transport $\delta\theta_{\text{Transport}}$ along the radiator bars is a function of a number of mechanisms. Some of these (e.g., small non-parallelism of the surfaces or a small

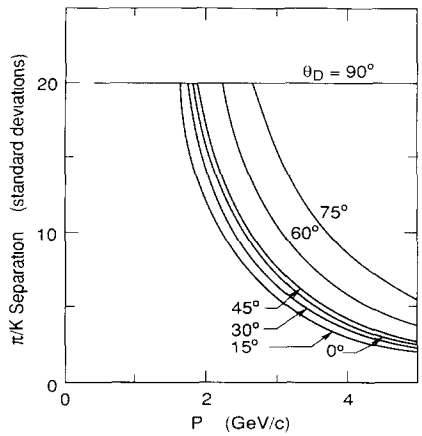

Fig. 9. The predicted π/K separation as a function of momentum in a DIRC counter with a detector resolution of 6.8 mrad. The lines show the dependence for a variety of track dip angles θ_D.

number of well defined changes in bar angle) can be calibrated out, in principle. Others (such as surface "waves" or variations in refractive index) could lead to emittance growth and must be strictly controlled. Fig. and surface quality specifications typical of optical components would be more than adequate. For the smearing calculation here, it will be assumed that quality can be sufficiently well controlled that $\delta\theta_{\text{Transport}}$ can be ignored.

– $\delta\theta_{\text{Detector}}$: The smearing of the photon angles due to measurement granularity comes from the size of the Cherenkov image (as formed by the bar dimensions) convoluted with the granularity of the photodetector surface, divided by the length from the radiator end to the detector. It is not "fundamental" but is driven by economics. For example, for a photon traveling in the y–z plane, if we assume a detector made up of closely packed 2 in. PMTs (with spatial resolution δy_{PMT}) located at 165 cm (L) from the end of the 1.23 cm thick radiator, the detector resolution would be 6.8 mrad.

The performance of any imaging Cherenkov is a strong function of momentum, of course, because the angular separation between particle species is such a rapidly varying function of momentum. The expected π/K separation versus momentum is shown in Fig. 9. There is a natural enhancement of the separation at the forward angles due primarily to the increasing number of photons detected. Since the asymmetric machines can only produce the fastest particles at large dip angles, the detector described above actually has over 5σ separation for all B factory tracks. Even a device with a detector resolution of 10 mrad would have over 4σ separation for all B factory tracks.

7. Comments on the detector model

A few comments now follow on choices made in the model detector and some possible changes to the model are indicated. Most of these issues are discussed in more detail elsewhere [3].

7.1. Penetration of the magnet poles pieces

The solution discussed above requires essentially complete azimuthal penetration of the pole pieces by the light bars. This requires an external support structure for the end "plug", of the magnet pole piece, with the photodetection surface probably lying inside the support structure. Though this is clearly an unusual requirement on the pole piece structure and requires a detailed engineering analysis, it seems possible to design such a structure. The best solution of all would be to find photodetectors with adequate performance that would operate in a magnetic field thus removing the necessity to penetrate the pole pieces.

7.2. Detector issues

The number of PMTs required for a DIRC is large and a major component of the cost. Essentially, the detector resolution specification "fixes" the number of pixels required to cover a certain solid angle. Pixels must be placed sufficiently far away from the radiator end to reach the required resolution. The size required for these pixels is dependent on the nature of the focusing system. For the non-focusing standoff system discussed above, there is a simple relationship between pixel size and the distance between the radiator end and the detector surface. Minimization of the detector cost, while keeping the track overlap problem under control, tends to lead to tubes in the 2 in. range, but most other considerations would argue for smaller pixel sizes.

In principle, a focusing system can be devised which will compensate for the finite size of the detector bar. This might allow the use of a rather small detection surface, with significantly smaller pixel size, if a detector which matches these needs can be found. Possible candidate detectors might be microchannel plate (MCP) PMTs; multianode PMTs [12,15]; and silicon photodetectors [13,14], and significant progress has been made in many of these areas in the last few years. However, at the moment we are not aware of any commercially available device of this type that meets all the necessary criteria.

8. Conclusion

The DIRC has many attractive features and appears to be extremely well matched to the require-

ments for a particle identification device at the B factory. Of course there are a number of potential problems that need to be addressed for the DIRC, and since it is a new device, a full scientific prototype is highly desirable. The number of photodetection pixels required is quite large (of order 10 000 or more), so the cost will probably be rather large (5–10M$). There is a "conventional" commercially available choice available for the photodetection surface (PMTs), although other techniques might be preferable if they become available. The most uncertain elements to manufacture are the radiator pieces. Though the finish specifications are not particularly severe by high-end optical industry standards, the pieces are very large and it will be a major challenge to produce them in the sizes required and still keep costs under control. R&D is now centered on radiator production and evaluation, photodetector evaluation and construction, and software studies, leading to the construction and testing of a physics prototype.

References

[1] SLAC-REP-373 (1991).
[2] For reviews, see e.g., B. Ratcliff, SLAC-PUB-5853 (1992), and
P. Coyle et al., SLAC-PUB-5594 (1991).
[3] B. Ratcliff, BaBar Note 92 (1992), SLAC-PUB-5946 (1992) and SLAC-PUB-6047 (1993).
[4] P. Baillon, Nucl. Instr. and Meth. A 238 (1985) 341;
S. Yellin, CRID analysis internal note.
[5] For a simple analytic treatment of image formation, see, B. Ratcliff, Presentation to the PEP-II Particle ID working group, July 1992.
[6] R.M. Bionta et al., Proc. 17th Rencontre de Moriond, 1982.
[7] G. Kettenring, Nucl. Instr. and Meth. 131 (1975) 451; manufacturers data, Rohm and Haas, Philadelphia, PA.
[8] R.P. Cargille Labs, Cedar Grove, NJ, USA.
[9] Fiberguide Industries, Stirling, NJ, USA.
[10] Melles Griot, Irving, CA, USA.
[11] A DIRC counter which is read out using only the time dimension has been proposed and simulated by M. Selen and K. Honscheid, see these Proceedings (1st Workshop on Ring Imaging Cherenkov Detectors, Bari, Italy, 1993) Nucl. Instr. and Meth. A 343 (1994) 306; Also CBX 92-116.
[12] For a discussion of tests of some of these devices see, e.g., C. Jeanney, DPhePE 91-07 (1991)
[13] See, for example, Advanced Photonics, Camarillo, CA.
[14] M. Atac et al., Nucl. Instr. and Meth. A 320 (1992) 155.
[15] G. Comby et al., these Proceedings (1st Workshop on Ring Imaging Cherenkov Detectors, Bari, Italy, 1993) Nucl. Instr. and Meth. A 343 (1994) 263.